Journal of Immunological Methods 465 (2019) 1–6

Contents lists available at ScienceDirect

Journal of Immunological Methods

journal homepage: www.elsevier.com/locate/jim

Research paper

Non-invasive dynamic monitoring initiation and growth of pancreatic tumor in the LSL-Kras$^{G12D/+}$;LSL-Trp53$^{R172H/+}$;Pdx-1-Cre (KPC) transgenic mouse model

Su Hu[a,b,1], Liang Pan[b,c,1], Junjie Shangguan[b], Matteo Figini[b], Aydin Eresen[b], Chong Sun[b,d], Bin Wang[b,e], Quanhong Ma[b], Chunhong Hu[a], Vahid Yaghmai[b,f], Yuri Velichko[b,f], Jia Yang[b,*], Zhuoli Zhang[b,f,*]

[a] Department of Radiology, The First Affiliated Hospital of Soochow University, Suzhou, Jiangsu 215006, China
[b] Department of Radiology, Feinberg School of Medicine, Northwestern University, Chicago, IL 60611, USA
[c] Department of Radiology, The Third Affiliated Hospital of Soochow University, Changzhou, Jiangsu 213003, China
[d] Department of Orthopedic, The Affiliated Hospital of Qingdao University, Qingdao, Shandong 266003, China
[e] Department of Hepatobiliary and Pancreatic Surgery, The Second Affiliated Hospital, Zhejiang University School of Medicine, Hangzhou 310009, China
[f] Robert H. Lurie Comprehensive Cancer Center, Chicago, IL 60611, USA

ARTICLE INFO

Keywords:
Pancreatic cancer
KPC mouse model
Tumorigenesis
Magnetic resonance imaging

ABSTRACT

The LSL-Kras$^{G12D/+}$;LSL-Trp53$^{R172H/+}$;Pdx-1-Cre (KPC) mouse is one of the most widely used transgenic models to evaluate tumor characteristics and to develop novel therapies for pancreatic ductal adenocarcinoma (PDAC). There is no report of the effective systemic evaluation of longitudinal KPC tumor imitation and growth. Therefore, we aimed to characterize the initiation and progression of pancreatic cancer in KPC mice using longitudinal multiparametric magnetic resonance imaging (MRI) approaches and overall survival. Ten KPC mice were used to develop spontaneous PDAC and monitored by MRI. Tumor growth was evaluated using weekly acquired MRI data. The relationship between diffusion-weighted MRI (DW-MRI) imaging biomarkers (apparent diffusion coefficient - ADC) and tumor fibrosis measurement by pathological methods was assessed by Pearson correlation coefficient. Six KPC mice developed spontaneously pancreatic tumors at the age of 20.0 ± 2.9 weeks with a relatively short life span (6.8 ± 1.8 weeks). The tumors could be detected by MRI with a minimum diameter of 3.88 ± 1.18 mm (range, 2.18–5.20 mm), showing a rapid growth curve according to both the longest diameter (1.63 ± 0.52 mm/week) and tumor volume (148.77 ± 80.87 mm^3)/week. Pathological results confirmed that the tumors display histopathological features of human pancreatic cancer. A strong correlation between ADC values and fibrosis measurements was observed ($R = -0.825$, $P = .043$). Our results show that the initiation and progression of pancreatic tumor in KPC mice can be evaluated by longitudinally non-invasive dynamic MRI approaches. The findings will be the fundamental KPC background data for developing novel therapeutic approaches, in particular for evaluation of response to novel treatments.

1. Introduction

Pancreatic ductal adenocarcinoma (PDAC) is predicted to become the second leading cause of cancer-related death in the United States by 2030 (Bekkali and Oppong, 2017; Renz et al., 2018). The overall 5-year survival rate of PDAC is only 5% with < 6 months of median survival (Cao et al., 2018). Although many advances in the understanding of molecular mechanisms involved pancreatic cancer pathogenesis have

Abbreviations: KPC, LSL-Kras$^{G12D/+}$;LSL-Trp53$^{R172H/+}$;Pdx-1-Cre; PDAC, Pancreatic Ductal Adenocarcinoma; MRI, Magnetic Resonance Imaging; ADC, Apparent Diffusion Coefficient; GEM, Genetically Engineered Mice; CT, Computed Tomography; PET, Positron-Emission Tomography; DWI, Diffusion-Weighted Imaging; T2W, T2-weighted; TSE, Turbo Spin Echo; TR, repetition time; TE, Echo time; ST, Slice Thickness; FA, Flip Angle; FOV, Field of View; T1W, T1-weighted; SE, Spin Echo; EPI, Echo Planar imagine; ROI, Region of Interest; H&E, Hematoxylin and Eosin; CK19, Cytokeratin 19; RECIST, Response Evaluation Criteria in Solid Tumors guidelines

* Corresponding authors at: Department of Radiology, Northwestern University, 737 N Michigan Ave, 16th Floor, Chicago, IL 60611, USA.
E-mail addresses: jia.yang@northwestern.edu (J. Yang), zhuoli-zhang@northwestern.edu (Z. Zhang).
[1] These two authors contributed equally to this work.

https://doi.org/10.1016/j.jim.2018.11.009
Received 23 October 2018; Received in revised form 19 November 2018; Accepted 19 November 2018
Available online 20 November 2018

been made over last four decades, further discovery and understanding of disease mechanism are necessary for improvement of diagnosis and treatment regimens (Torres et al., 2013). Therefore, development of preclinical animal models has vital importance for studying the underlying causes of tumor development, growth and dissemination of human PDAC, as well as developing the effective and novel treatment for this deadly malignancy (Bai et al., 2017; Golan et al., 2017; Partecke et al., 2011).

Currently, several mouse models of pancreatic cancer have been studied (Herreros-Villanueva et al., 2012; Ritelli et al., 2015). These include subcutaneously and/or orthotopically implanted xenografts of human tumor cells (Partecke et al., 2011). These models cannot either provide the role of immune mechanisms or resemble the biological characteristics of human pancreatic cancer (Partecke et al., 2011; Torres et al., 2013). More recently, genetically engineered mice (GEM) models that develop spontaneous PDAC have greatly advanced our understanding of pancreatic cancer pathogenesis and allowed the evaluation of promising diagnostic and therapeutic strategies (Torres et al., 2013). Several GEM models that accurately mimic the pathophysiological characteristics of human PDAC have been described (de Latouliere et al., 2016; Farr et al., 2017; Ijichi, 2011). In particular, the LSL-$Kras^{G12D/+}$;LSL-$Trp53^{R172H/+}$;Pdx-1-Cre, termed KPC mouse has attracted increasing attention, because it recapitulates the pathophysiological aspects and the biology features of human PDAC (Bai et al., 2017; Courtin et al., 2013; Hingorani et al., 2005).

Although histologic exams remain as the gold standard for monitoring tumor growth and metastasis formation, the collection of tissue samples are invasive inherently and will increase the number of animals required during the studies (Wu et al., 2014). Thus, a non-invasive method to monitor the tumor initiation and growth, and to evaluate the therapeutic response is highly desirable (Grimm et al., 2003). Several *in vivo* imaging modalities, such as computed tomography (CT), positron-emission tomography (PET), optical imaging, and ultrasound, have been developed for assessing tumor size and/or volume in animal models (Cao et al., 2008; Ritelli et al., 2015; Wu et al., 2014). Among them, MRI provides a powerful tool for preclinical research due to several combined advantage (Partecke et al., 2011). For instance, MRI offers better resolution and discrimination of soft tissues (Schmid et al., 2013), and is also capable of multi-faceted and multi-sequence imaging (Wang et al., 2017). Furthermore, tissue cellular density and/or tumor fibrosity can be easily monitored with quantitative sequences such as diffusion-weighted imaging (DWI) (Kobes et al., 2016).

In this study, we have further characterized pancreatic tumors arising in the KPC mouse model *in vivo*, describing both their patterns of initiation and growth using longitudinal multi-parametric MRI approaches. Our results will be the fundamental KPC background data for developing novel therapeutic approaches, in particular for evaluation of response to novel treatments.

2. Materials and methods

All studies were approved by the institutional animal care and use committee of Northwestern University and performed in accordance with National Institutes of Health guidelines.

2.1. Mice model

LSL-$Kras^{G12D/+}$, LSL-$Trp53^{R172H/+}$, and Pdx1-Cre mice were obtained from the Jackson Laboratory (Bar Harbor, ME, USA). To produce triple transgenic $Kras^{G12D}$;$Trp53^{R172}$;Pdx-1-Cre mice (KPC mice), double transgenic LSL-$Kras^{G12D/+}$;LSL-$Trp53^{R172/+}$ mice were first generated by cross-mating LSL-$Kras^{G12D/+}$ and LSL-$Trp53^{R172/+}$ mice, and then LSL-$Kras^{G12D/+}$; LSL-$Trp53^{R172/+}$ mice were further mated with transgenic Pdx-1-Cre mice (Fig. 1). All mice were genotyped in our laboratory following the protocols provided by Jackson lab. Ten KPC mice were used to generate spontaneous PDAC and monitored using high-resolution MRI approaches. The subjects were housed under clean conditions in the facilities of Laboratory Animal Services at the Northwestern University.

2.2. MRI protocol

The MRI studies were performed using a Bruker 7.0 T preclinical scanner (Clinscan, Bruker BioSpin, Ettlingen, Germany) with a commercial mouse coil (Clinscan, Bruker). For each mouse, imaging was performed fortnightly from approximately 8 weeks of age, increasing to weekly once the tumor was detected. The mice were anesthetized using a mixture of 2–3% isoflurane in oxygen at a rate of 1 L/min *via* an automatic delivery system (Isoflurane Vaporizer, Vaporizer Sales and Services, Rockmart, GA, USA). Each mouse was fixed in a supine position using a restraint apparatus. The depth of anesthesia was monitored by the respiratory rate and MRI sequences were triggered by this rate. Body temperature was continuously monitored using a thermometer and controlled using a water-bed heating system (SA Instruments, Stony Brook, NY, USA). For tumor localization, coronal T2-weighted (T2W) images (Turbo Spin Echo (TSE); Repetition time (TR): 1600 ms; Echo time (TE): 37 ms; slice thickness (ST): 1.0 mm; flip angle (FA): 180°; field of view (FOV): 36 × 28 mm^2) of 10 slices were acquired. Then, multi-parametric MRI were performed: (1) axial T1-weighted (T1W) images (Spin Echo (SE); TR: 867 ms; TE: 20 ms; ST: 0.7 mm; FA: 90°; FOV: 27 × 30 mm^2), (2) axial T2W images (TSE; TR: due to respiratory gating approx. 2100 ms; TE: 40 ms; ST: 0.5 mm; FA: 180°; FOV: 21 × 30 mm^2), (3) coronal T2W images (TSE; TR: due to respiratory gating approx. 2100 ms; TE: 40 ms; ST: 0.5 mm; FA: 180; FOV: 40 × 30 mm^2), (4) sagittal T2W images (TSE; TR: due to respiratory gating approx. 2500 ms; TE, 40 ms; ST: 0.5 mm; FA: 180; FOV: 24 × 30 mm^2), and (5) DW images (Echo Planar Imagine (EPI); TR: due to respiratory gating approx. 2700 ms; TE: 40 ms; ST: 1 mm; FA: 90°; FOV: 24 × 30 mm^2; b value = 0, and 800 s/mm^2). Both the T1W and T2W MRI images were acquired with fat suppression.

2.3. Imaging analysis

All MR images were analyzed by a radiologist with > 5 years of experience. However, difficult findings or images were always discussed with a senior radiologist. Tumor sizes including the longest diameter and tumor volume were measured with T2W images using ITK-SNAP software (v3.6.0), www.itksnap.org (Yushkevich et al., 2006). DW images were post-processed to generate ADC maps in Matlab R2016b (Mathworks, Natick, MA), and ADC was measured using ImageJ software (Rasband, W.S., ImageJ, U. S. National Institutes of Health, Bethesda, Maryland, USA, https://imagej.nih.gov/ij/, 1997–2016) (Schneider et al., 2012). Using axial T2-weighted images as reference, five ellipsoid region of interest (ROI) of approximately 5–15 mm^2 was drawn within the tumor solid part on the slice of apparent diffusion coefficient (ADC) maps in each mouse, avoiding regions with necrosis and artifacts. Then the average ADC value of tumor was calculated. ROIs were also drawn on the pancreatic tissues.

2.4. Histologic examinations

After longitudinal studies, the subjects were euthanized, and the pancreas tissue was dissected. The pancreases were inspected for grossly visible tumors and fixed in 4% paraformaldehyde for further histologic studies. Sections of 4 μm were stained with hematoxylin and eosin (H&E), anti-cytokeratin 19 (CK19) (DSHB TROMA III-C), anti-Ki67 (Thermo Fisher), and Masson's trichrome. Masson's trichrome stain was used to visualize the stromal matrix. Quantification was performed using ImageJ software at a high field magnification. Fibrotic stroma was depicted as blue-stained bands of collagen, and the tumor cells were identified by the stained nucleus. The percentage of fibrotic tissue was measured as: total fibrotic area/total tumor tissue

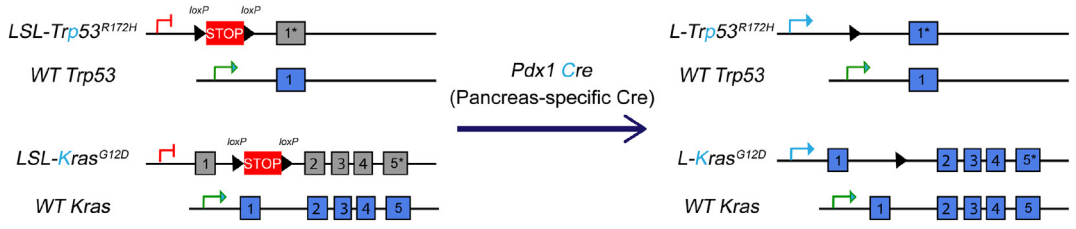

Fig. 1. Genetic strategy for generation of LSL-Kras$^{G12D/+}$;LSL-Trp53$^{R172H/+}$;Pdx-1-Cre (KPC) mouse model. Schematic representation of transgenic mice obtained from LSL-Kras$^{G12D/+}$ crossed with LSL-Trp53$^{R172/+}$ mice, and then double transgenic Kras^{G12D};Trp53^{R172} mice crossed with Pdx-1-Cre mice.

area × 100.

2.5. Statistical analysis

All statistical analyses were performed by using a statistical software package (SPSS, version 19; Chicago, IL, USA). Variables were summarized as mean ± standard deviation (SD). The difference of ADC values between pancreatic tissues and tumors was analyzed using student *t*-test. Pearson correlation coefficients were used to investigate the relationship between longest diameter and tumor volume, and between measurements of ADC values and corresponding histologic fibrosis measurements. $P < .05$ was considered significant.

3. Results

3.1. MRI findings of pancreatic tumor initiation and growth

Pancreatic tumor was detected by MRI in ten KPC mice. During experiment, two mice died during MRI scanning with anesthesia adjustments at week-4 and week-5 respectively. Two mice were excluded as veterinary suggested due to mouse bite each other with wounds. Six KPC mice were included in this study. The median age of onset was 20.0 ± 2.9 weeks (range 17 weeks to 25 weeks). Tumors could be clearly detected on the MR images when they reached a diameter ≥ 2.0 mm (average, 3.88 ± 1.18 mm).

In vivo pancreatic tumor growth rate was measured in real-time by the non-invasive MR imaging. Representative images (T1W, T2W, and ADC map) of dynamic changes with pancreatic tumor are shown from the same mouse in Fig. 2 A–I. The tumors manifested as homogeneous hypo-intensity on T1W, hyper-intensity on T2W at the early time points on MRI, and heterogeneous hyper-intensity on T2W images at later time points. The tumors demonstrated hypo-intensity on ADC maps.

The tumor volume was calculated by a semi-automatic image analysis on T2W images. The tumor growth curves including longest diameter and tumor volume are shown in Fig. 3 A, B. Both the longest diameter and tumor volume increased rapidly in KPC mice, with an average growth rate of 1.63 ± 0.52 mm in longest diameter and 148.77 ± 80.87 mm^3 in tumor volume per week. In addition, the measurements of longest diameter were compared to the results of tumor volume indicating a strong correlation ($R = 0.921$, $P < .001$) (Fig. 3 C).

KPC mice have a relatively short life span due to the pancreatic tumor burden. The median survival time was 26.8 ± 3.2 weeks after birth (Fig. 4 A) and 6.8 ± 1.8 weeks after tumor detection by MRI (Fig. 4 B).

3.2. Histologic findings of PDAC in KPC mice

Histology and immunohistochemistry were further conducted to identify the characteristics of pancreatic tumor in KPC mice. H&E staining slices confirmed that the excised mass was composed by tumor cells (Fig. 5 A). Staining for CK19 highlights the ductal differentiation of the pancreatic tumors (Fig. 5 B). The lesions also showed high expression level of Ki67 (Fig. 5 C). Masson's trichrome staining showed diffuse distribution of fibrotic tissue within the tumors (Fig. 5 D).

3.3. Correlation between MRI and histologic results

After the last time-point of MRI scan, the ADC measurements for pancreatic tissues and tumors were summarized and compared as

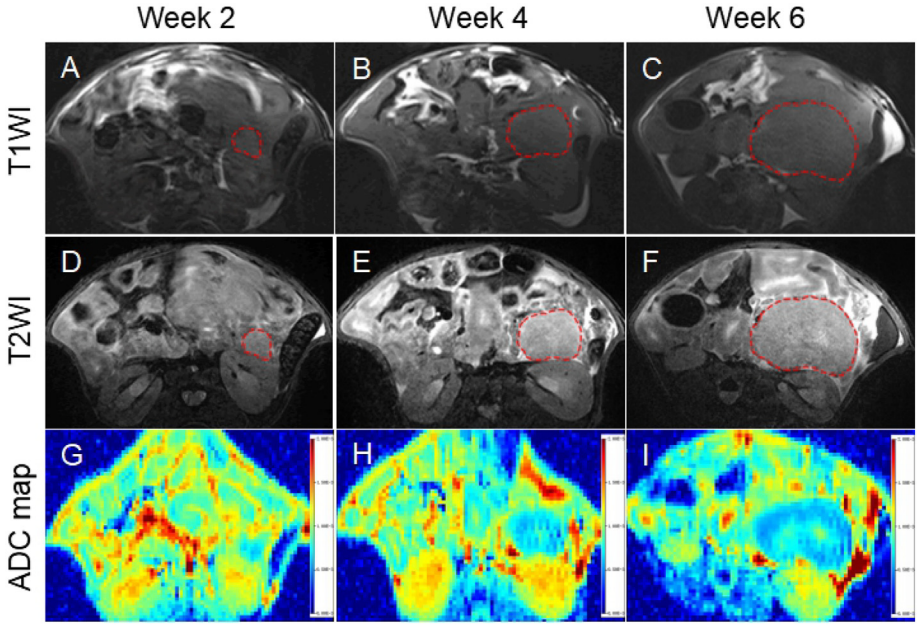

Fig. 2. Representative serial images with pancreatic cancer. The tumor showed homogeneous hypo-intense on T1-weighted image (A) and hyper-intense on T2-weighted image (D) with a diameter of 2.23 mm at two weeks. At four weeks, the tumor progressed rapidly with the diameter of 6.54 mm (B, E). At six weeks, the tumor showed homogeneous hypo-intense on T1-weighted image (C) and heterogeneous hyper-intense with small patchy necrosis on T2-weighted image (F). The tumor manifested as low-intensity on corresponding ADC maps (G, H, I).

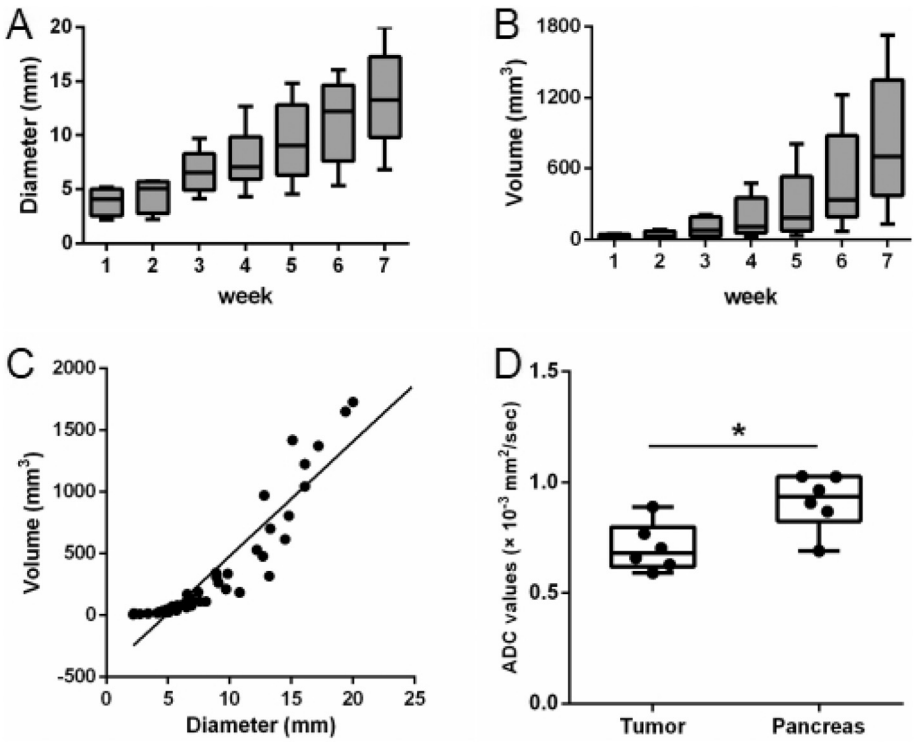

Fig. 3. Longitudinal monitoring and quantitatively measurements of pancreatic tumor growth in KPC mice. The longest diameter and tumor volume were measured weekly. The tumor showed an average growth rate of 1.63 ± 0.52 mm in longest diameter (A) and 148.77 ± 80.87 mm^3 in tumor volume (B) per week. A strong correlation was displayed between diameter-based and volume-based tumor size measurements (R = 0.921, $P < .001$, C). The bar graphs showed significant difference in ADC measurements between the tumors and pancreatic tissues ($P = .012$, D).

shown in Fig. 3 D. The average ADC values in KPC mouse tumors was $(0.71 \pm 0.10) \times 10^{-3}\,mm^2/s$, which was lower than that in KPC pancreatic tissues $(0.91 \pm 0.12 \times 10^{-3}\,mm^2/s)$ ($P = .012$). The average percentage of fibrotic tissue area measured on Masson's trichrome staining sections was 6.57%. Then, these data were compared with the ADC measurements of KPC mice tumors, and a strong correlation ($R = -0.825$, $P = .043$) between ADC values and fibrotic tissue area measurements was observed.

4. Discussion

The KPC mouse model has been widely utilized in pancreatic cancer research. This model is ideal for testing the efficacy of novel therapies due to KPC mouse mimics both the genetic and histologic changes of human PDAC (Chen et al., 2017; Olive et al., 2009). However, the current approaches to investigating pancreatic cancer pathophysiology and treatment are static and fail to present a dynamic view of tumor development (de Latouliere et al., 2016). Satisfactory non-invasive imaging has not yet been completely established for this transgenic model. In this study, MRI techniques were used to assess tumor onset, growth and characteristics of PDAC in KPC mice non-invasively and longitudinally. Our results demonstrate that MRI can be used for early detection of tumor lesion and accurate measurements of tumor development non-invasively. The KPC mouse model can develop all stages of pancreatic tumor spontaneously, from pancreatic intraepithelial neoplasia to invasive PDAC (Aeffner et al., 2016; Courtin et al., 2013). In the present study, the KPC mice developed pancreatic tumors with typical histological features of human PDAC. Our results reveal that small lesions with 3.88 ± 1.18 mm in diameter can be reliably visualized on high-resolution MRI with respiration triggering acquisition technology. However, KPC mice develop advanced PDAC from 2 to 3 months and have a median survival of approximately 5 months (Courtin et al., 2013; Ma and Saiyin, 2017), making detection of early-stage PDAC difficult. To detect tumor onset, we screened the KPC mice every 2 weeks starting at approximately 8 weeks of age and found that the primary tumor can be observed at a median age of 20.0 ± 2.9 weeks. MRI is thus highly useful for non-invasive screening and assessment of PDAC in KPC mice.

Furthermore, tumor progression can be monitored over time *via* MRI technique in the same animal. Thus, the number of required animals for longitudinal studies would be significantly reduced. Each mouse can be imaged at different time points and served as its own control (Partecke et al., 2011). However, to the best of our knowledge, *in vivo* assessment for pancreatic tumor development in KPC mice at 7 T had seldom been reported. Both tumor diameter and volume were

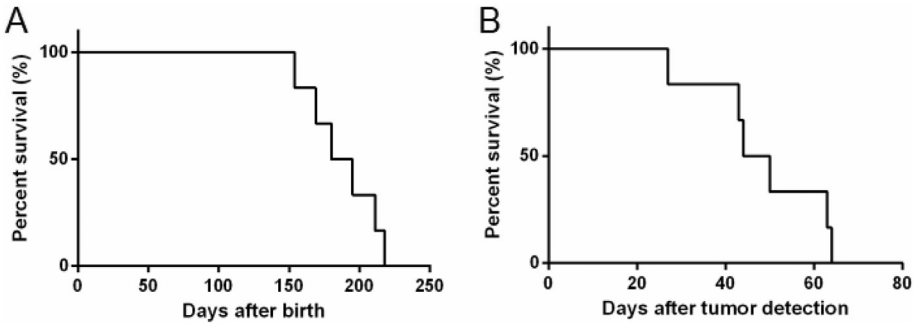

Fig. 4. Survival curves and histological analysis of pancreatic lesions in KPC mice. Kaplan-Meier plot of survival showed that the median survival time was 26.8 ± 3.2 weeks after birth (A), and 6.8 ± 1.8 weeks from tumor detection by MRI (B).

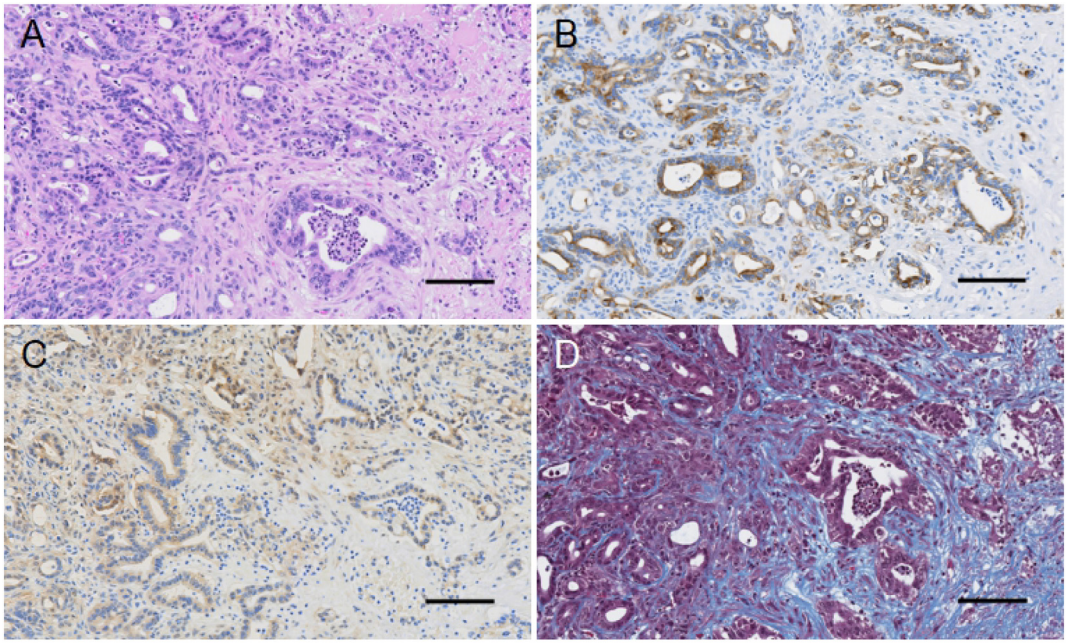

Fig. 5. Histological features of pancreatic tumor in KPC mice. Tumor cells and glandular are shown on H&E staining section (A). The ductal differentiation of the tumor are displayed on section staining for CK19 (B). Staining for Ki67 showed high expression of Ki67 (C). Masson-trichrome-staining section showed dense fibrotic tissue (blue stained bands) within the tumors (D). Scale bars = 100 μm. (For interpretation of the references to colour in this figure legend, the reader is referred to the web version of this article.)

measured longitudinally using T2W images, and then the tumor growth rate was analyzed. This study represents the effort dynamically to evaluate tumor development by MRI. Moreover, our results demonstrate that there is a strong correlation between measurements of diameter and tumor volume. Diameter measurement approach is the conventional imaging criteria for clinical evaluation of treatment response in cancer, which is widely known as the Response Evaluation Criteria in Solid Tumors guidelines (RECIST) (Eisenhauer et al., 2009; Suzuki et al., 2008). Its wide use is due to the relative ease of use and requiring less time of analysis compared to measurement of tumor volume.

Tumor desmoplasia is one of the common pathological features of human PDAC, characterized by dense fibrotic connective tissue that penetrates and envelopes the tumor(Li et al., 2012). These extracellular matrix is related with tumor progression, metastasis, and drug resistance (Farr et al., 2017). Hence, it is significantly important to characterize the tumor fibrosis to predict tumor grade and response to treatments. Hereby, DW-MRI has served as a non-invasive biomarker to measure fibrosis level of PDAC. The results demonstrated a significant difference between the ADC values of the tumor and pancreatic tissue. This can be explained by the accumulation of fibrotic tissue, which may be associated with restricted motion of the water protons (Farr et al., 2017).

The current study had several limitations. First, the tumor margin is difficult to delineate sometimes, which may result in a deviation of measurements of tumor size. This limitation, however, can be corrected by the use of a contrast agent and additional scan. Furthermore, the field of view used in our study only allowed visualization of the upper abdomen, which excludes the possible metastasis in other sites.

5. Conclusions

Our study demonstrated that MRI can be used to identify the pancreatic tumor and monitor the tumor progression, and DWI may be helpful to characterize the tumor fibrosis in KPC mouse model. These results are the fundamental KPC background data for developing novel therapeutic approaches, in particular for evaluation of response to novel treatments.

Declaration of conflicting interest

The Authors declare that there is no conflict of interest.

Funding source

This work was supported by the National Institutes of Health, National Cancer Institute grants R01CA196967 and R01CA209886.

References

Aeffner, F., Martin, N.T., Peljto, M., Black, J.C., Major, J.K., Jangani, M., Ports, M.O., Krueger, J.S., Young, G.D., 2016. Quantitative assessment of pancreatic cancer precursor lesions in IHC-stained tissue with a tissue image analysis platform. Lab. Investig. 96, 1327.

Bai, Z., Shi, Y., Wang, J., Qiu, L., Teng, G., Zhang, F., Yang, X., 2017. Multi-modality imaging-monitored creation of rat orthotopic pancreatic head cancer with obstructive jaundice. Oncotarget 8, 54277–54284. https://doi.org/10.18632/oncotarget.17347.

Bekkali, N.L.H., Oppong, K.W., 2017. Pancreatic ductal adenocarcinoma epidemiology and risk assessment: could we prevent? Possibility for an early diagnosis. Endosc. Ultrasound 6, S58–S61. https://doi.org/10.4103/eus.eus_60_17.

Cao, X., Jia, G., Zhang, T., Yang, M., Wang, B., Wassenaar, P.A., Cheng, H., Knopp, M.V., Sun, D., 2008. Non-invasive MRI tumor imaging and synergistic anticancer effect of HSP90 inhibitor and glycolysis inhibitor in RIP1-Tag2 transgenic pancreatic tumor model. Cancer Chemother. Pharmacol. 62, 985–994. https://doi.org/10.1007/s00280-008-0688-8.

Cao, X.-Y., Zhang, X.-X., Yang, M.-W., Hu, L.-P., Jiang, S.-H., Tian, G.-A., Zhu, L.-L., Li, Q., Sun, Y.-W., Zhang, Z.-G., 2018. Aberrant upregulation of KLK10 promotes metastasis via enhancement of EMT and FAK/SRC/ERK axis in PDAC. Biochem. Biophys. Res. Commun. 499, 584–593. https://doi.org/10.1016/j.bbrc.2018.03.194.

Chen, K., Qian, W., Jiang, Z., Cheng, L., Li, J., Sun, L., Zhou, C., Gao, L., Lei, M., Yan, B., Cao, J., Duan, W., Ma, Q., 2017. Metformin suppresses cancer initiation and progression in genetic mouse models of pancreatic cancer. Mol. Cancer 16, 131. https://doi.org/10.1186/s12943-017-0701-0.

Courtin, A., Richards, F.M., Bapiro, T.E., Bramhall, J.L., Neesse, A., Cook, N., Krippendorff, B.-F., Tuveson, D.A., Jodrell, D.I., 2013. Anti-Tumour Efficacy of Capecitabine in a Genetically Engineered Mouse Model of Pancreatic Cancer. PLoS One 8, e67330. https://doi.org/10.1371/journal.pone.0067330.

Eisenhauer, E.A., Therasse, P., Bogaerts, J., Schwartz, L.H., Sargent, D., Ford, R., Dancey, J., Arbuck, S., Gwyther, S., Mooney, M., Rubinstein, L., Shankar, L., Dodd, L., Kaplan, R., Lacombe, D., Verweij, J., 2009. New response evaluation criteria in solid tumours: revised RECIST guideline (version 1.1). Eur. J. Cancer 45, 228–247. https://doi.org/

10.1016/j.ejca.2008.10.026.
Farr, N., Wang, Y., D'Andrea, S., Gravelle, K.M., Hwang, J.H., Lee, D., 2017. Noninvasive characterization of pancreatic tumor mouse models using magnetic resonance imaging. Cancer Med. 6, 1082–1090. https://doi.org/10.1002/cam4.1062.
Golan, T., Stossel, C., Schvimer, M., Atias, D., Halperin, S., Buzhor, E., Raitses-Gurevich, M., Cohen, K., Pri-Chen, S., Wilson, J., Denroche, R.E., Lungu, I., Bartlett, J.M.S., Mbabaali, F., Yarden, Y., Nataraj, N.B., Gallinger, S., Berger, R., 2017. Pancreatic cancer ascites xenograft–an expeditious model mirroring advanced therapeutic resistant disease. Oncotarget 8, 40778–40790. https://doi.org/10.18632/oncotarget.17253.
Grimm, J., Potthast, A., Wunder, A., Moore, A., 2003. Magnetic resonance imaging of the pancreas and pancreatic tumors in a mouse orthotopic model of human cancer. Int. J. Cancer 106, 806–811. https://doi.org/10.1002/ijc.11281.
Herreros-Villanueva, M., Hijona, E., Cosme, A., Bujanda, L., 2012. Mouse models of pancreatic cancer. World J. Gastroenterol. 18, 1286–1294. https://doi.org/10.3748/wjg.v18.i12.1286.
Hingorani, S.R., Wang, L., Multani, A.S., Combs, C., Deramaudt, T.B., Hruban, R.H., Rustgi, A.K., Chang, S., Tuveson, D.A., 2005. Trp53R172H and KrasG12D cooperate to promote chromosomal instability and widely metastatic pancreatic ductal adenocarcinoma in mice. Cancer Cell 7, 469–483. https://doi.org/10.1016/j.ccr.2005.04.023.
Ijichi, H., 2011. Genetically-engineered mouse models for pancreatic cancer: advances and current limitations. World J. Clin. Oncol. 2, 195–202. https://doi.org/10.5306/wjco.v2.i5.195.
Kobes, J.E., Daryaei, I., Howison, C.M., Bontrager, J.G., Sirianni, R.W., Meuillet, E.J., Pagel, M.D., 2016. Improved treatment of pancreatic cancer with drug delivery nanoparticles loaded with a novel AKT/PDK1 inhibitor. Pancreas 45, 1158–1166. https://doi.org/10.1097/MPA.0000000000000607.
de Latouliere, L., Manni, I., Iacobini, C., Pugliese, G., Grazi, G.L., Perri, P., Cappello, P., Novelli, F., Menini, S., Piaggio, G., 2016. A bioluminescent mouse model of proliferation to highlight early stages of pancreatic cancer: a suitable tool for preclinical studies. Ann. Anat. Anat. Anzeiger 207, 2–8. https://doi.org/10.1016/j.aanat.2015.11.010.
Li, W., Zhang, Z., Nicolai, J., Yang, G.-Y., Omary, R.A., Larson, A.C., 2012. Magnetization transfer MRI in pancreatic cancer xenograft models. Magn. Reson. Med. 68, 1291–1297. https://doi.org/10.1002/mrm.24127.
Ma, L., Saiyin, H., 2017. LSL-Kras(G12D); LSL-Trp53(R172H/+); Ink4(flox/+); Ptf1/p48-Cre mice are an applicable model for locally invasive and metastatic pancreatic cancer. PLoS One 12, e0176844. https://doi.org/10.1371/journal.pone.0176844.
Olive, K.P., Jacobetz, M.A., Davidson, C.J., Gopinathan, A., McIntyre, D., Honess, D., Madhu, B., Goldgraben, M.A., Caldwell, M.E., Allard, D., Frese, K.K., Denicola, G., Feig, C., Combs, C., Winter, S.P., Ireland, H., Reichelt, S., Howat, W.J., Chang, A., Dhara, M., Wang, L., Rückert, F., Grützmann, R., Pilarsky, C., Izeradjene, K., Hingorani, S.R., Huang, P., Davies, S.E., Plunkett, W., Egorin, M., Hruban, R.H., Whitebread, N., McGovern, K., Adams, J., Iacobuzio-Donahue, C., Griffiths, J., Tuveson, D.A., 2009. Inhibition of hedgehog signaling enhances delivery of chemotherapy in a mouse model of pancreatic cancer. Science 324, 1457–1461. https://doi.org/10.1126/science.1171362.
Partecke, I.L., Kaeding, A., Sendler, M., Albers, N., Kühn, J.-P., Speerforck, S., Roese, S., Seubert, F., Diedrich, S., Kuehn, S., Weiss, U.F., Mayerle, J., Lerch, M.M., Hadlich, S., Hosten, N., Heidecke, C.-D., Puls, R., von Bernstorff, W., 2011. In vivo imaging of pancreatic tumours and liver metastases using 7 Tesla MRI in a murine orthotopic pancreatic cancer model and a liver metastases model. BMC Cancer 11, 40. https://doi.org/10.1186/1471-2407-11-40.
Renz, B.W., Takahashi, R., Tanaka, T., Macchini, M., Hayakawa, Y., Dantes, Z., Maurer, H.C., Chen, X., Jiang, Z., Westphalen, C.B., Ilmer, M., Valenti, G., Mohanta, S.K., Habenicht, A.J.R., Middelhoff, M., Chu, T., Nagar, K., Tailor, Y., Casadei, R., Di Marco, M., Kleespies, A., Friedman, R.A., Remotti, H., Reichert, M., Worthley, D.L., Neumann, J., Werner, J., Iuga, A.C., Olive, K.P., Wang, T.C., 2018. β2 Adrenergic-neurotrophin feedforward loop promotes pancreatic cancer. Cancer Cell 33https://doi.org/10.1016/j.ccell.2017.11.007. 75–90.e7.
Ritelli, R., Ngalani Ngaleu, R., Bontempi, P., Dandrea, M., Nicolato, E., Boschi, F., Fiorini, S., Calderan, L., Scarpa, A., Marzola, P., 2015. Pancreatic cancer growth using magnetic resonance and bioluminescence imaging. Magn. Reson. Imaging 33, 592–599. https://doi.org/10.1016/j.mri.2015.02.017.
Schmid, A., Braumüller, H., Wehrl, H.F., Röcken, M., Pichler, B.J., 2013. Non-invasive monitoring of pancreatic tumor progression in the RIP1-Tag2 mouse by magnetic resonance imaging. Mol. Imaging Biol. 15, 186–193. https://doi.org/10.1007/s11307-012-0548-0.
Schneider, C.A., Rasband, W.S., Eliceiri, K.W., 2012. NIH image to ImageJ: 25 years of image analysis. Nat. Methods 9, 671–675.
Suzuki, C., Jacobsson, H., Hatschek, T., Torkzad, M.R., Bodén, K., Eriksson-Alm, Y., Berg, E., Fujii, H., Kubo, A., Blomqvist, L., 2008. Radiologic measurements of tumor response to treatment: practical approaches and limitations. Radiographics 28, 329–344. https://doi.org/10.1148/rg.282075068.
Torres, M.P., Rachagani, S., Souchek, J.J., Mallya, K., Johansson, S.L., Batra, S.K., 2013. Novel pancreatic cancer cell lines derived from genetically engineered mouse models of spontaneous pancreatic adenocarcinoma: applications in diagnosis and therapy. PLoS One 8, e80580. https://doi.org/10.1371/journal.pone.0080580.
Wang, R., Guo, Q., Chen, Y., Gao, Y., Wu, L., Hu, B., Jiang, L., 2017. Efficacy of subthreshold focused ultrasound irradiation against pancreatic cancer xenografts evaluated using magnetic resonance imaging. Oncotarget 8, 80453–80460. https://doi.org/10.18632/oncotarget.19241.
Wu, L., Wang, C., Yao, X., Liu, K., Xu, Y., Zhang, H., Fu, C., Wang, X., Li, Y., 2014. Application of 3.0 Tesla magnetic resonance imaging for diagnosis in the orthotopic nude mouse model of pancreatic cancer. Exp. Anim. 63, 403–413. https://doi.org/10.1538/expanim.63.403.
Yushkevich, P.A., Piven, J., Hazlett, H.C., Smith, R.G., Ho, S., Gee, J.C., Gerig, G., 2006. User-guided 3D active contour segmentation of anatomical structures: significantly improved efficiency and reliability. NeuroImage 31, 1116–1128. https://doi.org/10.1016/j.neuroimage.2006.01.015.